CIRCULATION AND REACTION HOTSPOTS IN AN INTERTIDAL SALT MARSH: A MODELING STUDY

Mathilde Hagens[1] and Christof Meile[2*]

AUTHORS: [1]Faculty of Geosciences, Utrecht University, P.O.Box 80021, 3508 TA Utrecht, The Netherlands; [2]Department of Marine Sciences, University of Georgia, Athens, Georgia, 30602; *cmeile@uga.edu
REFERENCE: *Proceedings of the 2011 Georgia Water Resources Conference*, held April 11–13, 2011, at the University of Georgia.

Abstract. Intertidal salt marshes are highly productive, dynamic ecosystems at the interface between the land and the ocean that can play a significant role in reducing nutrient loading to the coastal ocean. To assess the spatio-temporal patterns in salt marsh biogeochemistry, a reactive transport model describing tidally-driven flow as well as solute dynamics across a marsh cross-section was developed.

Porewater residence times were computed to identify zones of rapid fluid exchange. Model simulations suggest the presence of circulation hotspots at the creek bank and the upland-marsh transition zone, whose intensity varies over a tidal cycle. The location and magnitude of these regions of rapid fluid exchange depend on the tidal amplitude, and on the presence or absence of terrestrial groundwater input from the upland.

The introduction of oxygenated creek water to the marsh subsurface also promotes biogeochemical reactions and hence may be important for regulating the marsh's filter function. Reaction hotspots are located at the interface between chemically distinct water bodies such as upland-derived groundwater and the intruding tidal creek water. As a result, these hotspots develop at the fringes of circulation hotspots, but are not identical to the locations of highest infiltration. The relative importance of reaction hotspots varies substantially with tidal amplitude and their presence has important implications for the placement of monitoring wells in field studies.

INTRODUCTION

Salt marshes along the southeastern US coast belong to the most productive ecosystems of the world (Dame and Kenny 1986), with an estimated net primary productivity of circa 700 gC m^{-2} yr^{-1} (Mendelssohn and Morris 2000), generally limited by N availability (Howarth 1988). Salt marshes export both organic and inorganic materials to coastal waters (Valiela et al. 1978) and intercept nutrients derived from upland waters (Valiela et al. 2000). Therefore, they may play a significant role in reducing increased nutrient input caused by anthropogenic activity, preventing eutrophication of the coastal ocean (Vitousek et al. 1997).

Flow in salt marshes is complex as the variability in tidal elevation leads to alternating saturated and unsaturated conditions. In addition, sediment permeability and compressibility (Wilson and Gardner 2006), vegetation (Ursino et al. 2004) and salt marsh geomorphology (Gardner 2005, 2007) influence the magnitude and location of fluid exchange and subsequent salt marsh nutrient export (Moore et al. 2006; Krest et al. 2000).

The fate and export of nutrients in salt marshes is controlled by nutrient loading, flooding frequency and hydraulic gradient (Morris 2000) and biogeochemical processes (Vörösmarty and Loder 1994) and depends on the relative magnitude of flow and transformations. Water residence times may serve as a measure to distinguish between zones dominated by transport and by biogeochemical reactions. Porewater residence times in salt marshes have been shown to vary significantly, ranging from less than 1 hour to circa 2 days in the top few centimeters of sediments from North Inlet, South Carolina (Bollinger and Moore 1993), indicating the presence of zones of rapid fluid exchange. In these zones, the introduction of oxygenated water may promote reaction hotspots: regions of limited extent that account for a high percentage of total biogeochemical turnover. Similarly, tidal dynamics may lead to 'hot moments', short time periods with significantly higher biogeochemical turnover rates compared to intervening time periods (McClain et al. 2003).

In this study, we assess the presence, importance and physical controls on the formation of hotspots and hot moments. Because modeling reaction hotspot and hot moment formation requires a spatio-temporally resolved assessment of advective and dispersive transport, as well as biogeochemical transformation rates, we use a 2-D variably saturated reactive transport model. Our study focuses on conditions representative for salt marshes in the Southeastern United States, with a transition from an upland/hammock environment to a tidal creek that connects to the coastal ocean.

METHODS

The model domain describes an upland - marsh - tidal creek system typical for a salt marsh at the Georgia coast (Fig. 1). The marsh is regularly inundated by creek water due to semidiurnal tides, which are mimicked by creek water levels varying as a sinusoidal function with a period of 12 hours. The domain boundaries are set at the middle of the tidal creek where symmetry conditions apply, and at 10 m into the upland. For simulations where the upland boundary represents the middle of a hammock, symmetry conditions are imposed, while for settings where the marsh is connected to the main land, a freshwater head and a known fluid composition are defined, reflecting the inflow of terrestrial groundwater. At the bottom of the domain, a no flow/no flux boundary is chosen, assuming an impermeable layer. On the top of the domain, boundary conditions depend on flow direction and inundation. In case of surface exposure and unsaturated conditions, a no flow/no flux condition is applied. When the surface is exposed and saturated, atmospheric pressure is imposed, while during surface inundation, hydrostatic pressure is imposed. In the latter two cases, an advective flow is assigned for solutes, with the water composition depending on whether fluid moves to or from the subsurface.

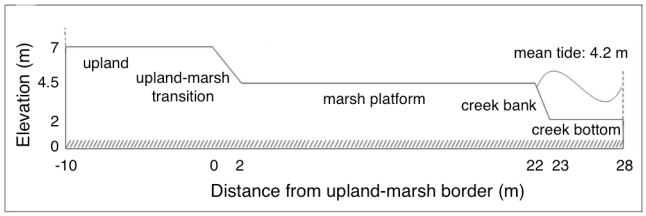

Figure 1: Site description of model domain

Fluid flow was modeled with Richards' equation, adapted for changes in total stress due to changes in tidal elevation (Reeves et al. 2000) and assuming constant density:

$$\left(\rho S_w S_{op} + \rho\theta_s \frac{\partial S_w}{\partial P}\right)\frac{\partial P}{\partial t} = \nabla\left[\frac{k_r k\rho}{\eta}\left(\nabla P - \rho g\right)\right] + \rho S_w \zeta S_{op}\frac{\partial \sigma}{\partial t} \quad (1)$$

where S_w is saturation (-), P is pressure (Pa), k_r is relative permeability (-) and σ is total stress (Pa). S_w and k_r are computed via constitutive relationships (Gardner 1958):

$$S_w = \frac{\theta_r - \left(\theta_s - \theta_r\right)e^{\alpha \min(0,H_p)}}{\theta_s} \quad (2a)$$

$$k_r = e^{\alpha \min(0,H_p)} \quad (2b)$$

where H_p is the pressure head (m). Values and definitions of constants are given in Table 1.

Table 1: Physical parameters. Sources: [1]Wilson and Gardner (2006); [2]Gardner and Wilson (2006); [3]Schultz and Ruppel (2002).

Property	Symbol	Value
Porewater density	ρ	1020 kg m^{-3}
Residual water content	θ_r	0.255[3]
Storativity	S_{op}	8.20.10^{-7} Pa^{-1} [3]
Porosity	θ_s	0.425 [2]
Permeability	k	10^{-11} m^2 [3]
Gravimetric constant	g	9.81 m s^{-2}
Loading efficiency	ζ	1 [1]
Inverse capillary rise	α	1 m^{-1} [1]
Dynamic viscosity	η	0.001 Pa s^{-1}

Solute dynamics were coupled to Richards' equation via the Darcy velocity $u = -\frac{k_r k}{\eta}\nabla\left(P - \rho g\right)$ and expressed by:

$$\theta\rho\frac{\partial c}{\partial t} + \left(1-\theta_s\right)\rho_s\frac{\partial c_s}{\partial t} = -u\nabla c + \nabla\left(\theta\rho D_s \nabla C\right) + \theta\rho R_L \quad (3)$$

where D_s is the diffusion-dispersion tensor that depends on flow velocities and longitudinal and transverse dispersivities (Scheidegger 1961), θ is the fluid fraction, c is the solute concentration, with the subscript s denoting a solid, ρ_s is the bulk density, set to 2650 kg m^{-3} and R_L denotes the net reaction rate. A baseline scenario was parameterized with a longitudinal dispersivity of 0.1 m, a transverse dispersivity of 0.01 m, a tidal amplitude (TA) representative for Georgia salt marshes of 0.75 m and a mean tidal elevation located 0.3 m below the marsh platform. To determine the residence time of the water in the marsh, porewater age was implemented as a solute having a unit reaction rate (R_L = 1 s^{-1}; Goode 1996). In simulations of interacting water bodies, $R_L = k\, c_1\, c_2$, where $c_{1,2}$ are the concentrations of two reactive tracers, and the rate constant k is set to 1.59·10^{-4} (mol m^{-3})$^{-1}$ s^{-1}. Simulations were performed using the finite element software COMSOL v3.5a with a maximum time step of 60 seconds and a varying mesh size with smallest elements (area = 0.05 m^2) along the upper boundaries.

RESULTS

Variations in fluid flow

Simulations for the hammock - marsh - creek system reveal two dominant tidally-driven flow directions in the marsh subsurface. Flow is landwards and upwards towards the unsaturated zone during mid-rising and high tide, and seawards and downwards during mid-falling and low tide (Fig. 2), indicating two flow reversals within the aquifer over a tidal cycle. These

transitions have a time lag with respect to the slack tides in the creek water. Highest seepage velocities are found at the intersection of the water table with the surface. As a consequence, 65.2% of the net marsh porewater discharge occurs at the creek bank across the topographic drop between marsh platform and tidal creek (Fig. 3a). In contrast to the upland, where in the absence of rain events S_w shows little variation, saturation on the temporarily inundated marsh platform varies significantly, with a minimum S_w of 0.78 during low tide at the marsh platform - creek bank intersection.

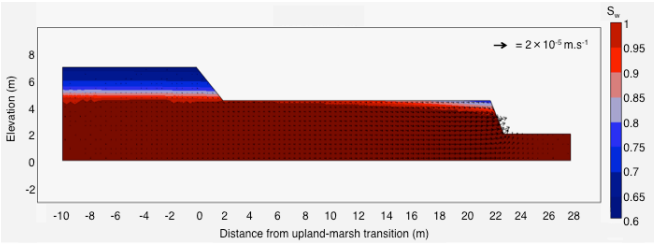

Figure 2: Flow pattern and saturation (S_w) at low tide.

The net outflow, i.e. the difference between in- and outflow integrated over the boundary, varies as a function of time, with patterns differing substantially between the upland-marsh transition, marsh platform, creek bank and creek bottom (Fig. 3a). By assuming a third dimension into the plane along the creek of unit length, flows are expressed in m^3 per m and time. The total flow shows that a transition from net inflow to net outflow occurs at t=1.5 hrs, while the reverse change takes place at t=7.8 hrs. The timing of these transitions coincides with the reversal in flow patterns in the aquifer described above. The contributions of the separate surfaces over a tidal cycle show that net inflow occurs across the upland-marsh transition and marsh platform, while net outflow takes place across the creek bank and creek bottom. This means that, in a net sense, creek water enters the marsh subsurface at the landward side of the marsh and porewater is lost at the seaward side, indicating that the general flow direction within the aquifer is towards the tidal creek. The total net outflow across the several boundaries per tidal cycle is 0.02 m^3 m^{-1} for the upland-marsh boundary, 0.09 m^3 m^{-1} for the marsh platform, 0.17 m^3 m^{-1} for the creek bottom and 0.53 m^3 m^{-1} for the creek bank, summing up to a total of 0.81 m^3 m^{-1}. For the range tested (TA = 0.4 to 1.45 m) the total volume of fluid being exchanged each tidal cycle depends linearly on tidal amplitude (Fig. 3b).

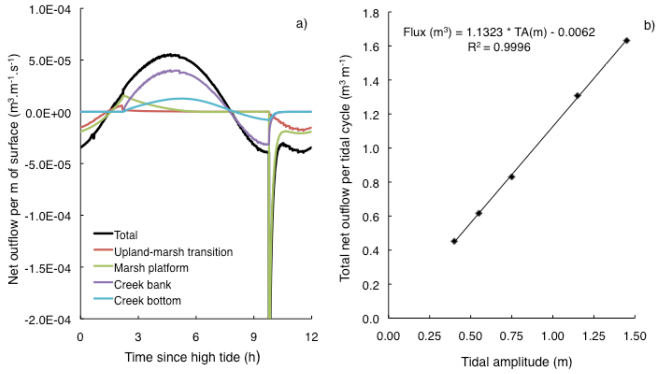

Figure 3: a) Net outflow (m^3 m^{-1} s^{-1}) for the baseline simulation; the inflow peak extends to -8·10^{-4} m^3 m^{-1} s^{-1}. b) Total fluid exchange volume (m^3 m^{-1}) per tidal cycle as a function of tidal amplitude.

Marsh porewater age

Simulations of porewater age over several tidal cycles show the development of two zones subject to rapid flushing (Fig. 4). The youngest water can be found at the intersection between upland and marsh platform, where inflow of creek water exceeds seepage (Fig. 3a), hence porewater around this landward hotspot is always younger than 12 hours. At the second circulation hotspot, along the creek bank around mean tidal elevation, inflow over a tidal cycle is significant but is exceeded by outflow (Fig. 3a). As a result, relatively old water is found during low tide, after maximum creek bank seepage, while during high tide, much younger porewater is observed. When upland groundwater inflow is included, the effect of tidal forcing on the flow dynamics in the marsh decreases (left insets Fig. 4).

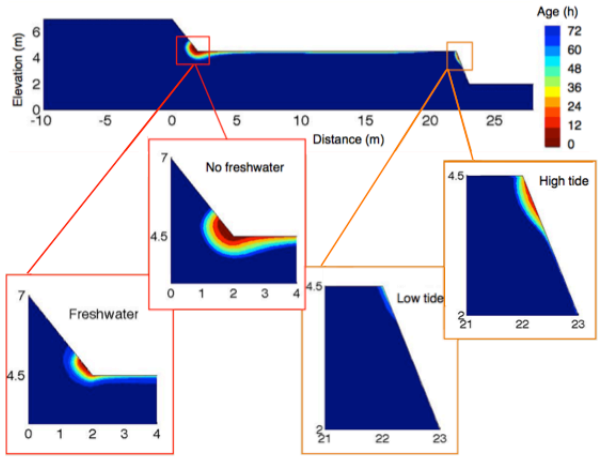

Figure 4: Age distribution of porewater at high tide. Ages exceeding 72 hrs are depicted uniformly in dark blue. The insets highlight the differences in porewater ages in the presence and absence of terrestrial groundwater input (left) and during different tidal stages (right).

Tracer reactivity

Terrestrially derived groundwater differs in composition from tidal creek water. To account for the mixing of these two distinct water bodies, we simulated a tracer brought in via groundwater that reacts with a tracer entering the marsh via the creek water (Fig. 5). In this simulation two reaction hotspots form, of which the seaward one has a different location (x=23 m) compared to the seaward circulation hotspot (Fig. 4). This indicates that no fresh groundwater reaches the location of the seaward circulation hotspot. In contrast, the concurrence of the landward reaction hotspot (x=2 m) with the landward circulation hotspot from Fig. 4 indicates that this hotspot is dominated by the dynamic interplay of creek water and groundwater.

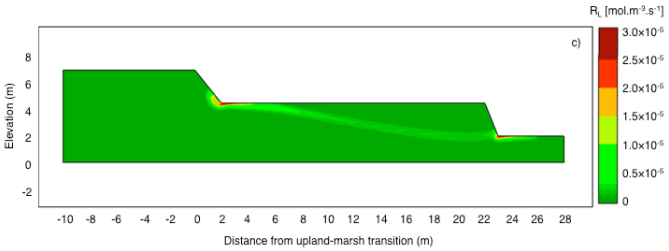

Figure 5: Reaction rate (mol m^{-3} s^{-1}) between groundwater and creek water associated reactive tracers at high tide.

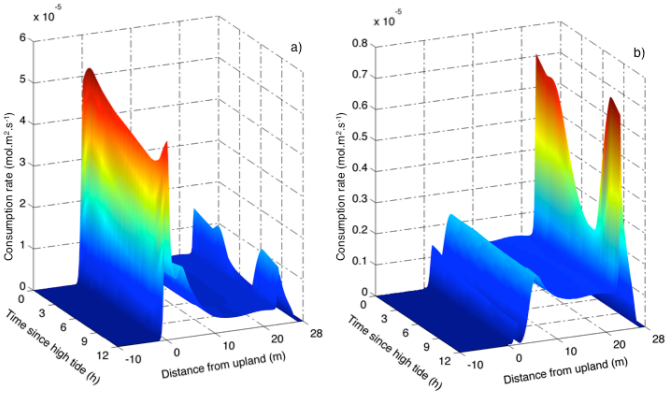

Figure 6: Depth-integrated reaction rates (mol m^{-2} s^{-1}) between the two tracers for TA=1.45 m (a) and 0.40 m (b) over a tidal cycle and across the domain.

To reflect natural tidal variability, TA was varied linearly from spring (TA=1.45 m) to neap (TA=0.40 m) and back to spring over 14 days. The temporal variability in the depth-integrated reaction rates (Fig. 6) between spring and neap conditions indicates that tidal flushing shapes the reaction rate pattern at both hotspots, as highest reaction rates are found just after maximum infiltration rates. At spring tide (Fig. 6a), reaction rates at the landward hotspot are approximately 50 times higher than during neap tide (Fig. 6b), reflecting the shorter inundation time of the upland - marsh system at neap tide.

DISCUSSION

Tidal forcing leads to flow reversals in the salt marsh subsurface. The lag in the changes in net flow direction compared to slack tide indicates the complex nature of flow dynamics in the marsh aquifer. The fluid exchange volume of 0.81 m^3 m^{-1} for the baseline scenario is significantly higher than the 0.31 m^3 m^{-1} that Wilson and Gardner (2006) computed in a similar study. Major differences are the absence of an upland-marsh transition in their study and that the total outflow volume was estimated based on the difference in fluid volume in the model domain between high tide and low tide, rather than the transition between net into outflow. By applying their method on the baseline scenario, a volume of 0.67 m^3 m^{-1} was computed. Field estimates of fluid exchange fluxes show a wide variation in results, ranging from 0.0039-0.014 m^3 m^{-1} of creek bank using seepage meters (Whiting and Childers 1989) to 0.31-0.54 m^3 m^{-1} using Ra isotopes (Krest et al. 2000). These lower values are likely reflecting the chosen positions of the measurement wells, as Whiting and Childers (1989) placed their wells below the low tide line. This may miss the highest seepage velocities and result in the underestimation of the true seepage, highlighting the importance of the seepage meter placement.

When the marsh platform is inundated at high tide, fluid exchange volume depends strongly on tidal amplitudes (Fig. 3b). Because the marsh platform is horizontal, the trend in Fig. 3b reflects that an increase in TA both increases the length of upland-marsh transition surface (Fig. 1) that gets inundated during rising tide and stimulates discharge from the exposed creek bank during falling tide.

Zones subject to rapid flushing affect salt marsh biogeochemistry in that they are regularly supplied with significant amounts of water having a different, more oxidized chemical signature than marsh porewater (e.g. Porubsky et al. 2010). Although the total net volume infiltrated per tidal cycle via the marsh platform is higher than the infiltration across the upland-marsh transition (0.38 m^3 m^{-1} and 0.14 m^3 m^{-1}, respectively), the inflow per surface area for the upland-marsh transition is much higher, i.e. 0.26 m^3 m^{-2} compared to 0.02 m^3 m^{-2}, explaining the location of the landward hotspot. The circulation hotspot at the creek bank reflects the highest in- and outflow velocities around the mean tide line.

Reaction hotspots can be associated with but are not identical to zones subject to rapid flushing. Rather, it is the mixing between distinct water masses - marsh porewater, upland-derived groundwater and tidal creek water - that promotes biogeochemical interactions. The simulations representative of groundwater entering the marsh aquifer (Fig. 5) indicate that at the landward circulation hotspot a mixing zone of e.g. reduced and oxidized water bodies is formed that promotes a reaction hotspot at the fringe of the zone of enhanced creek water input. The creek bank circulation hotspot, however, does not result in a reaction zone of similar extent, because the flow dynamics cause the upland-derived groundwater to largely bypass that region. Changing tidal amplitude (Fig. 6a, b) does not only affect the amount of water being renewed via infiltration and seepage across the marsh surface, but it also influences the inflow of terrestrial groundwater, as an increase in tidal amplitude leads to the tidal signal being propagated further inland. Since reactivity at neap tide at the landward reaction hotspot is only slightly higher compared to the surrounding marsh platform, this hotspot is also a hot moment when considering spring-neap variations in tidal forcing.

CONCLUSIONS

Computed flow patterns show that, averaged over a tidal cycle, creek water enters the marsh subsurface at the landward side of the marsh and porewater is lost at the seaward side. The transitions from net inflow to net outflow and vice versa have a time lag compared to the slack tides, indicating that the flow dynamics in the marsh aquifer are complex and cannot be linked directly to the elevation of the tidal creek. Porewater residence time simulations suggest the presence of two circulation hotspots at the loci of highest infiltration fluxes into the marsh aquifer.

The inclusion of inflowing upland-derived groundwater containing a reactive tracer promotes two reaction hotspots. The seaward one does not coincide with the circulation hotspot because of the prevalent flow patterns. Lunar variations in tidal amplitude mainly affect the landward hotspot, due to enhanced flushing with increasing tidal amplitude. Model simulations highlight the need for an experimental assessment of these zones of high reactivity to quantify their impact on the marsh potential to control and mitigate nutrient export to the coastal ocean.

ACKNOWLEDGEMENTS

We would like to thank A. Wilson for helpful discussions. This work has been supported by the National Science Foundation (OCE06-20959 and OCE-0928784). The views expressed herein do not necessarily reflect the views of NSF.

REFERENCES

Bollinger, M.S., W.S. Moore (1993). Evaluation of salt marsh hydrology using radium as a tracer. *Geochimica et Cosmochimica Acta* 57, pp. 2203-2212.

Dame, R.F., P.D. Kenny (1986). Variability of *Spartina alterniflora* primary production in the euhaline North Inlet estuary. *Marine Ecology Progress Series* 32, pp. 71-80.

Gardner, W.R. (1958). Some steady state solutions of unsaturated moisture flow equations to applications to evaporation from a water table. *Soil Science* 82, pp. 228-232.

Gardner, L.R. (2005). Role of geomorphic and hydraulic parameters in governing pore water seepage from salt marsh sediments. *Water Resources Research* 41, W07010, doi: 10.1029/2004WR003671.

Gardner, L.R. (2007). Role of stratigraphy in governing pore water seepage from salt marsh sediments. *Water Resources Research* 43, W07502, doi: 10.1029/2006WR005338.

Goode, D.J. (1996). Direct simulation of groundwater age. *Water Resources Research* 32(2), pp. 289-296.

Howarth, R.W. (1988). Nutrient limitation of net primary production in marine ecosystems. *Annual Review of Ecology and Systematics* 19, pp. 89-110.

Krest, J.M., W.S. Moore, L.R. Gardner, J.T. Morris (2000). Marsh nutrient export supplied by groundwater discharge: evidence from radium measurements. *Global Biogeochemical Cycles* 14(1), pp. 167-176.

McClain, M.E., E.W. Boyer, C.L. Dent, S.E. Gergel, N.B. Grimm, P.M. Groffman, S.C. Hart, J.W. Harvey, C.A. Johnston, E. Mayorga, W.H. McDowell, G. Pinay (2003). Biogeochemical hotspots and hot moments at the interface of terrestrial and aquatic ecosystems. *Ecosystems* 6, pp. 301-312.

Mendelssohn, I.A., J.T. Morris (2000). Ecophysiological controls on the productivity of *Spartina alterniflora* Loisel. In: Concepts and Controversies in Tidal Marsh Ecology. Kluwer Academic Publishers, Dordrecht, The Netherlands, doi: 10.1007/0-306-47534-0_3.

Moore, W.S., J.O. Blanton, S.B. Joye (2006). Estimates of flushing times, submarine groundwater discharge, and nutrient fluxes to Okatee Estuary, South

Carolina. *Journal of Geophysical Research* 111, C09006, doi: 10.1029/2005JC003041.

Morris, J.T. (2000). Effect of sea-level anomalies on estuarine processes. In: Estuarine science: A synthetic approach to research and practice. Island Press, Washington, DC, United States of America, 539 pp.

Porubsky, W.P., S.B. Joye, W.S. Moore, K. Tuncay, C. Meile (2010). Field measurements and modeling of groundwater flow and biogeochemistry at Moses Hammock, a backbarrier island on the Georgia coast. *Biogeochemistry*, doi: 10.1007/s10533-010-9484-8.

Reeves, H.W., P.M. Thibodeau, R.G. Underwood, L.R. Gardner (2000). Incorporation of total stress changes into the ground water model SUTRA. *Ground Water* 38(1), pp. 89-98.

Scheidegger, A. (1961). General theory of dispersion in porous media. *Journal of Geophysical Research* 66, pp. 3273-3278.

Schultz, G., C. Ruppel (2002). Constraints on hydraulic parameters and implications for groundwater flux across the upland-estuary interface. *Journal of Hydrology* 260, pp. 255-269.

Ursino, N., S. Silvestri, M. Marani. (2004). Subsurface flow and vegetation patterns in tidal environments. *Water Resources Research* 40, W05115, doi: 10.1029/2003WR002702.

Valiela, I., M.L. Cole, J. McClelland, J. Hauxwell, J. Cebrian, S.B. Joye (2000). Role of salt marshes as part of coastal landscapes. In: Concepts and Controversies in Tidal Marsh Ecology. Kluwer Academic Publishers, Dordrecht, The Netherlands, doi: 10.1007/0-306-47534-0_3.

Valiela, I., J.M. Teal, S. Volkmann, D. Shafer, E.J. Carpenter (1978). Nutrient and particulate fluxes in a salt marsh ecosystem: tidal exchanges and inputs by precipitation and groundwater. *Limnology and Oceanography* 23(4), pp. 798-812.

Vitousek, P.M., J.D. Aber, R.W. Howarth, G.E. Likens, P.A. Matson, D.W. Schindler, W.H. Schlesinger, D.G. Tilman (1997). Human alteration of the global nitrogen cycle: sources and consequences. *Ecological Applications* 7(3), pp. 737-750.

Vörösmarty, C.J., T.C. Loder III (1994). Spring-neap tidal contrasts and nutrient dynamics in a marsh-dominated estuary. *Estuaries* 17(3), pp. 537-551.

Wilson, A.M., L.R. Gardner (2006). Tidally driven groundwater flow and solute exchange in a marsh: numerical solutions. *Water Resources Research* 42, W01405, doi: 10.1029/2005WR004302.

Whiting, G.J., D.L. Childers (1989). Subtidal advective water flux as a potentially important nutrient input to southeastern U.S.A. saltmarsh estuaries. *Estuarine, Coastal and Shelf Science* 28, pp. 417-431.